

Paulo Durão · Isabel Bento · André T. Fernandes  
Eduardo P. Melo · Peter F. Lindley · Lígia O. Martins

## Perturbations of the T1 copper site in the CotA laccase from *Bacillus subtilis*: structural, biochemical, enzymatic and stability studies

Received: 2 February 2006 / Accepted: 21 March 2006 / Published online: 21 April 2006  
© SBIC 2006

**Abstract** Site-directed mutagenesis has been used to replace Met502 in CotA laccase by the residues leucine and phenylalanine. X-ray structural comparison of M502L and M502F mutants with the wild-type CotA shows that the geometry of the T1 copper site is maintained as well as the overall fold of the proteins. The replacement of the weak so-called axial ligand of the T1 site leads to an increase in the redox potential by approximately 100 mV relative to that of the wild-type enzyme ( $E^0 = 455$  mV). However the M502L mutant exhibits a twofold to fourfold decrease in the  $k_{\text{cat}}$  values for the all substrates tested and the catalytic activity in M502F is even more severely compromised; 10% activity and 0.15–0.05% for the non-phenolic substrates and for the phenolic substrates tested when compared with the wild-type enzyme. T1 copper depletion is a key event in the inactivation and thus it is a determinant of the thermodynamic stability of wild-type and mutant proteins. Whilst the unfolding of the tertiary structure in the wild-type enzyme is a two-state process displaying a midpoint at a guanidinium hydrochloride concentration of 4.6 M and a free-energy exchange in water of 10 kcal/mol, the unfolding for both mutant enzymes is clearly not a two-state process. At 1.9 M guanidinium hydrochloride, half of the molecules are in an intermediate conformation, only slightly less stable than the native state (approximately 1.4 kcal/mol). The T1 copper centre clearly plays a key role, from the structural, catalytic and stability viewpoints, in the regulation of CotA laccase activity.

**Keywords** Laccases · T1 Cu site · Site-directed mutagenesis · Redox potential · Enzyme stability

### Introduction

Laccases are members of the multicopper oxidase family of enzymes that includes ascorbate oxidase (L-ascorbate oxygen oxidoreductase, EC 1.10.3.3) and ceruloplasmin [Fe(II) oxygen oxidoreductase, EC 1.16.3.1] [1, 2]. They are potential biocatalysts for diverse biotechnological applications [3, 4], mainly owing to their high relative non-specific oxidation capacity, the lack of a requirement for cofactors and the use of readily available oxygen as an electron acceptor. Redox biocatalysts are highly sought after because of the selectivity, controllability and economy of their reactions, in comparison with conventional chemical reactions. Moreover, biocatalyst-based processes require less energy and minimize the amount of waste produced, whilst at the same time being able to improve the quality and functional specifications of products. Recently, we undertook a multidisciplinary study of the CotA laccase from *Bacillus subtilis* as a model bacterial laccase system. CotA is a thermoactive and intrinsically thermostable enzyme [5]. X-ray studies have shown that the enzyme has a typical 3-domain laccase fold [6] with a T1 mononuclear copper centre in domain 3 and a trinuclear copper cluster (two T3 ions and a T2 copper ion) located between domains 1 and 3, and have given insights regarding the role of 2,2'-azinobis(3-ethylbenzothiazoline-6-sulfonic acid) (ABTS) as an oxidative mediator [7]. Moreover, studies involving structural intermediates of O<sub>2</sub> reduction have provided a new model mechanism for the dioxygen reduction in multicopper oxidases [8]. Such fundamental studies have been aimed at clarifying, at the molecular level, the catalytic activity and stability of these enzymes and the design of laccases that better match biotechnological applications by protein engineering techniques.

P. Durão · I. Bento · A. T. Fernandes · P. F. Lindley  
L. O. Martins (✉)  
Instituto de Tecnologia Química e Biológica,  
Universidade Nova de Lisboa, Av. da República,  
2781-901 Oeiras, Portugal  
E-mail: lmartins@itqb.unl.pt  
Tel.: +351-1-214469534  
Fax: +351-1-214411277

E. P. Melo  
Center of Molecular and Structural Biomedicine,  
Universidade do Algarve, Campus de Gambelas,  
8005-139 Faro, Portugal

The catalytic rate-limiting step in laccases is considered to be the oxidation of substrate at the T1 site, most probably controlled by the redox potential difference between this site and the trinuclear site [9]. Redox potentials exhibited by laccases span a broad range of values from 400 mV for plant laccases to 790 mV for some fungal laccases [10]. The conserved coordinating amino acids for the T1 copper site are two histidines and a cysteine, and the natural variations occur in the so-called axial position with a single interaction from a methionine being the most common arrangement. Fungal laccases have non-coordinating phenylalanine or leucine at this position and these may contribute, at least in part, to the high  $E^0$  observed in these enzymes, although other elements of the protein matrix are known to affect this important parameter of the T1 Cu centre [11]. The present study utilizes site-directed mutagenesis to examine how the replacement of a weakly coordinating methionine of the T1 mononuclear copper by the non-coordinating residues phenylalanine and leucine affect the structure and the redox potential of this centre and how these mutations affect the enzymatic properties,  $k_{\text{cat}}$  and  $K_{\text{m}}$ , of the enzyme and also its overall thermodynamic stability. This information will assist the development of strategies targeted at the improvement of laccases as biocatalysts.

## Materials and methods

### Construction of CotA mutants

Single amino acid substitutions in the T1 Cu centre were created using the QuickChange site-directed mutagenesis kit (Stratagene). Plasmid pLOM10 (containing the wild-type *cotA* sequence) was used as a template [5] and the primers

*cotA*-MLd (5'-GCATGAAGACTATGACCTGATGAGACCGATGG-3') and

*cotA*-MLr (5'-CCATCGGTCTCATCAGGTCATAGTCTTCATGC-3')

were used to generate the M502L. The primers

*cotA*-MFd (5'-GAAGACTATGACTTCATGAGACCGATG-3') and

*cotA*-MFr (5'-CATCGGTCTCATGAAGTCATAGTCTTC-3')

were used to generate the M502F mutation. The presence of the desired mutations in the resulting plasmids, pLOM13 (carrying the M502L point mutation) and pLOM52 (bearing the M502F point mutation), and the absence of unwanted mutations in other regions of the insert were confirmed by DNA sequence analysis. Plasmids pLOM13 and pLOM52 were transformed into *Escherichia coli* Tuner (DE3) strains (Novagen) to obtain strains AH3522 and LOM401, respectively.

### Overproduction and purification of wild type and M502L and M502F mutants

Strains AH3517 (containing pLOM10 [10]), AH3522 and LOM401 were grown in Luria–Bertani medium supplemented with ampicillin (100 µg/mL) at 25 °C. Growth was followed until the midlog phase ( $\text{OD}_{600}=0.6$ ), at which time 0.1 mM isopropyl- $\beta$ -D-thiogalactopyranoside and 0.25 mM  $\text{CuCl}_2$  were added to the culture medium. Incubation was continued for a further 4–6 h. Cell harvesting and disruption were performed as described by Martins et al. [5]. Proteins were purified by using a two-step purification protocol procedure as previously described [8]. Purified enzyme samples were prepared by incubation with 250 µM  $\text{CuCl}_2$  for 1 h at room temperature in 20 mM tris(hydroxymethyl)aminomethane (Tris) HCl buffer with 0.2 M NaCl, pH 7.6. The excess copper was removed by passing the solutions through a Sephadex G25 column (PD 10 columns, Amersham Pharmacia Biotech) that had been equilibrated with the same buffer. Purified enzymes were stored at  $-20$  °C until use.

### Crystallization and X-ray data collection

Crystals of both mutants were obtained from a crystallization solution containing 12% 2-propanol, 12% of poly(ethylene glycol) 4000, 0.1 M sodium citrate pH 5.5 and a protein concentration of about 5 mg/mL, using the vapour diffusion method. Pale-blue crystals appeared within 2 days at room temperature. Data collection was performed at the European Synchrotron Radiation Facility (ESRF), Grenoble, France, using beam line ID29. Two data sets were collected, one from each mutant, at  $-163$  °C, using a cryogenic solution that contained 20% of glycerol plus the crystallization solution. Details of the data collection are given in Table 1. Both data sets were processed and scaled with the programs DENZO and SCALEPACK from the HKL suite [12].

### Structure solution and refinement

The structure was determined by molecular replacement (MOLREP from the CCP4 program suite [13]) with the structure of the native protein (PDB code 1GSK) as a search model, but with copper ions and solvent molecules omitted and the side chain of residue 502 truncated at the  $\beta$ -carbon atom. In each case there was one well-discriminated solution with correlation coefficients of 0.71 and an  $R_{\text{factor}}$  of 0.35 for both the M502L and the M502F mutants. After five cycles of refinement with REFMAC [14] the electron density maps,  $2F_o - F_c$ , calculated for both mutants clearly revealed the positions of the four copper atoms. The electron density also showed the side chain for Leu502, and for Phe502, in the M502L and M502F mutants, respectively. Repeated

**Table 1** Data collection and refinement statistics

	M502L	M502F
<b>Data collection statistics</b>		
Beam line at ESRF	ID29	ID29
Wavelength (Å)	0.9756	0.9756
Detector	ADSC Q210 2D	ADSC Q210 2D
Distance	190	225
Resolution (Å)	2.05	2.3
Space group	<i>P</i> <sub>3</sub> 21	<i>P</i> <sub>3</sub> 21
Cell parameters (Å)		
<i>a</i>	101.45	101.97
<i>c</i>	135.85	136.11
Mosaicity (degrees)	0.2	0.3
Oscillation range (degrees)	60	94
Oscillation angle (degrees)	1.0	0.5
No. of unique <i>hkl</i> <sup>a</sup>	51,273 (5,068)	36,587 (3,616)
Completeness (%) <sup>a</sup>	100.0 (100.0)	99.3 (99.7)
<i>I</i> / $\sigma$ ( <i>I</i> ) <sup>a</sup>	17.2 (2.6)	19.4 (5.8)
<i>R</i> <sub>sym</sub> <sup>a</sup>	0.076 (0.531)	0.081 (0.282)
Multiplicity <sup>a</sup>	3.7 (3.7)	5.1 (5.1)
<b>Refinement</b>		
No. of protein atoms	4,086	4,095
No. of solvent atoms	458	434
No. of hetero atoms	4Cu + 2O + 4GOL	4Cu + 2O + 3GOL
Final <i>R</i> factor	0.16	0.15
Final free <i>R</i> factor	0.195 (5.1%)	0.184 (5.0%)
Mean <i>B</i> values (Å <sup>2</sup> )		
Protein	27.3	21.8
Solvent	37.8	31.1
Overall	28.5	22.3
Estimated overall coordinate uncertainty (Å) <sup>b</sup>	0.08	0.09
Distance deviations <sup>c</sup>		
Bond distances (Å)	0.02	0.02
Bond angles (Å)	1.44	1.52
Planar groups (Å)	0.01	0.01
Chiral volume deviation (Å <sup>3</sup> )	0.108	0.133
<b>Quality of models</b>		
Overall <i>G</i> factor	0	−0.1
Ramachandran analysis [% (no.)]		
Favourable	87.3 (370)	86.3 (366)
Additional	11.6 (49)	12.7 (54)
Generous	0.7 (3)	0.5 (2)
Disallowed	0.5 (2)	0.5 (2)

The *G* factor and Ramachandran analysis [16] were determined by PROCHECK [17]

<sup>a</sup>Values in parentheses refer to the highest-resolution shells as follows: M502L (2.12–2.05 Å); M502F (2.38–2.30 Å)

<sup>b</sup>Based on maximum likelihood

<sup>c</sup>Root-mean-square deviations from standard values

cycles of model building with the COOT program [15] and maximum-likelihood refinement with REFMAC resulted in final models with good stereochemistry and acceptable agreement residuals (Table 1). The overall structural models of both mutants were then compared with the structure of the native CotA, using the program ESCET [18].

### Enzyme assays

The laccase-catalysed oxidation reactions of ABTS, potassium ferrocyanoferrate (II) [K<sub>4</sub>(FeCN<sub>6</sub>)], syringaldazine (SGZ) and 2,6-dimethoxyphenol (2,6-DMP) were photometrically monitored with either a Nicolet Evolution 300 spectrophotometer from Thermo Industries or a Molecular Devices Spectra Max 340 microplate reader with a 96-well plate. The oxidation reactions of ABTS, K<sub>4</sub>(FeCN<sub>6</sub>), SGZ and 2,6-DMP were followed at 420 nm ( $\epsilon = 36,000 \text{ M}^{-1} \text{ cm}^{-1}$ ), 405 nm ( $\epsilon = 900 \text{ M}^{-1} \text{ cm}^{-1}$ ), 530 nm ( $\epsilon = 65,000 \text{ M}^{-1} \text{ cm}^{-1}$ ) and 468 nm

( $\epsilon = 49,600 \text{ M}^{-1} \text{ cm}^{-1}$ ), respectively. Oxidations were determined by using Britton–Robinson (BR) buffer (100 mM phosphoric acid, 100 mM boric acid and 100 mM acetic acid mixture with 0.5 M NaOH to the desired pH). The effect of pH on the enzyme activity was determined at 37 °C for the different substrates, in BR buffer (pH 3–10). The reaction mixtures contained 1 mM ABTS, 1 mM K<sub>4</sub>(FeCN<sub>6</sub>), 0.1 mM SGZ or 1 mM 2,6-DMP. Kinetics parameters were determined at 37 °C. The reaction mixtures contained ABTS (10–200  $\mu\text{M}$ , pH 4), K<sub>4</sub>(FeCN<sub>6</sub>) (10–200  $\mu\text{M}$ , pH 6), SGZ (1–100  $\mu\text{M}$ , pH 7) and 2,6-DMP (10–200  $\mu\text{M}$ , pH 7). The initial reaction rates were obtained from the linear portion of the progress curve. Kinetics data were determined from Lineweaver–Burk plots assuming that simple Michaelis–Menten kinetics was followed. All enzymatic assays were performed at least in triplicate. The protein concentration was measured by using the absorption band at 280 nm ( $\epsilon_{280} = 84,739 \text{ M}^{-1} \text{ cm}^{-1}$ ) or the Bradford assay using bovine serum albumin [19] as a standard.

## UV-vis spectra

UV-vis spectra were recorded using a Nicolet Evolution 300 spectrophotometer from Thermo Industries.

## Redox titrations

Redox titrations were performed at 25 °C, and pH 7.6, under an argon atmosphere, and were monitored by visible spectroscopy (300–900 nm), using a Shimadzu Multispec-1501 spectrophotometer. The reaction mixture contained 25–50 µM enzyme in 20 mM Tris-HCl buffer, pH 7.6, with 0.2 M NaCl and also the following mediators: 10 µM final concentration of dimethyl-*p*-phenylenediamine (+344 mV), monocarboxylic acid ferrocene (+530 mV), 1,1'-dicarboxylic acid ferrocene (+644 mV) and Fe(II/III) Tris-(1,10-phenanthroline) (+1,070 mV). Potassium hexachloroiridate(IV) was used as an oxidant and sodium dithionite as a reductant. The redox potential measurements were performed with a combined silver/silver chloride electrode, calibrated with a quinhydrone saturated solution at pH 7.0. The redox potentials are quoted against the standard hydrogen electrode. The reduction potentials were found to be reproducible within ±10 mV.

## Thermodynamic stability

Steady-state fluorescence was measured with a Carry Eclipse spectrofluorimeter using 280 nm as the excitation wavelength. CotA laccase and single mutants were in 20 mM Tris-HCl buffer at pH 7.6 with 200 mM NaCl. Several fluorescence signals can be used to monitor the unfolding transitions of proteins, such as steady-state fluorescence intensity, emission maximum and fluorescence anisotropy. Currently fluorescence intensity (total intensity by integrating the emission at different wavelengths or intensity at a specific wavelength) is mostly used and appropriately measured as it is directly related to the mole fraction of the states of the protein [20]. For some cases such as the enzymes under study, fluorescence intensity cannot be used because there is no significant discernible difference between the signals from macroscopic states that characterize unfolding transitions. Although, fluorescence intensity changes cannot be used, the emission maximum shifts to longer wavelengths upon unfolding when tryptophan residues become exposed to the high polarity of the water molecules (the enzyme emission maximum shifts from 330 to 354 nm upon unfolding). To monitor unfolding of the enzymes under study using fluorescence, a combination of two signals was used: fluorescence intensity and emission maximum. The use of the emission maximum might skew slightly the tracking of the population of states towards the more intensely emitting state [20, 21], but the use of these two signals was the only approach able to provide accurate data within the transition region. First, the spectra were normalized (dividing by

the intensity at the maximum of emission) to reflect clearly the shift in the emission maximum. Second, the wavelength at which the relative fluorescence intensity (intensity relative to the maximum) changes more significantly was selected (370 nm for CotA laccase and mutants) and the relative fluorescence intensity at this wavelength was used to monitor unfolding of CotA laccase and single mutants. Further details are given in the “Appendix”.

The thermodynamic stability was also evaluated based on enzymatic activity and absorbance at 600 nm in the presence of different concentrations of guanidinium hydrochloride (GdnHCl). The absorbance at 600 nm was measured in the presence of different GdnHCl concentrations (0–3 M), by using 123 µM CotA in 20 mM Tris-HCl pH 7.6 buffer with 200 mM NaCl. Enzymatic activity was measured in the same GdnHCl concentration range, following the oxidation of SGZ at 530 nm in the same buffer by using 0.015 µM CotA, 0.29 µM M502L and 0.30 µM M502F, respectively. These measurements were done in a 96-well-plate Spectra Max 384 spectrophotometer from Molecular Devices.

## Other methods

The amount of copper bound to the protein was determined through the trichloroacetic acid/bicinchoninic acid method of Brenner and Harris [22] and confirmed by atomic absorption (Chemical Analysis Facility, Instituto Superior Técnico, Universidade Técnica de Lisboa).

---

## Results and discussion

### Characterization of the axial variants in CotA laccase

The site-directed replacement of Met502, an axial ligand of the T1 copper site, by the non-coordinating residues leucine and phenylalanine resulted in enzymes that show the same chromatographic pattern during purification when compared with that of wild-type CotA laccase. Preparations were judged to be homogeneous by the observation of a single band on a Coomassie Blue stained sodium dodecyl sulfate polyacrylamide electrophoresis gel. Copper incorporation of wild-type CotA laccase was followed by the increase in absorbance at 600 nm, showing that the proteins, as purified, present an appreciable copper depletion. To ensure that copper depletion was minimized, the purified proteins samples were incubated for at least 1 h with excess copper, which was removed by passing the solution through a Sephadex-G25 column. Copper content measurements revealed a stoichiometry number close to 4 Cu per protein for the mutant M502L and M502F proteins, ensuring that all four coppers anions required to exert enzyme activity were incorporated into the active site. In con-

trast, the wild-type CotA laccase was not completely loaded with copper. On average, samples contained  $2.01 \pm 0.47$  Cu per protein. Incomplete metal incorporation was also observed in previous studies with CotA laccase [5–8], and as a consequence copper in a stoichiometry of 4:1 (copper-to-protein ratio) was added to the protein solutions. Nevertheless, samples of this latter protein were intense blue when compared with M502L and M502F mutant proteins, correlating with the higher signal intensity of the T1 Cu as monitored by the peak absorbance at 600 nm (Fig. 1). The sequential addition of the oxidizing agent, iridate, up to 10 times excess to the solutions of M502L and M502F proteins did not increase the band intensity at 600 nm, ruling out the hypothesis of the T1 Cu being in the reduced state in these isolated enzymes. Under the conditions tested, we

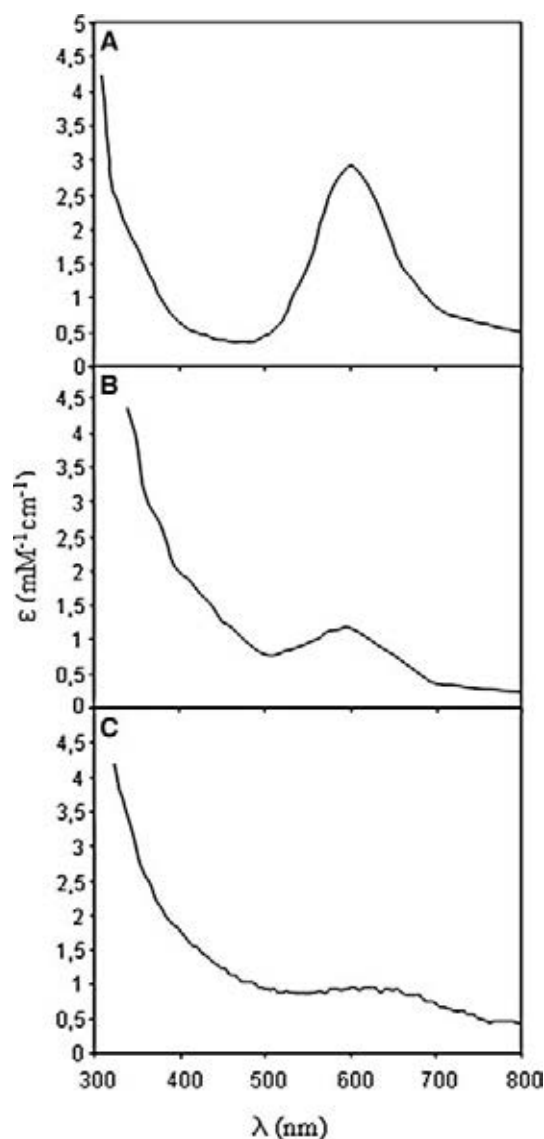


**Fig. 1** UV-vis spectra of wild-type recombinant CotA laccase (a), compared with that of M502L (b) and M502F (c) mutants. Spectra were recorded in 20 mM tris(hydroxymethyl)aminomethane HCl, pH 7.6, with 0.2 mM NaCl

had assumed that mutant enzymes were fully Cu loaded with oxidized T1 Cu. Comparison of different spectra shows the absence of a 330-nm band (Fig. 1) in any of the protein preparations. This band is indicative of the presence of a hydroxyl group bridging the type 3 copper ions [10]. In the wild-type CotA laccase our most recent studies indicate that the “isolated” enzyme has a dioxygen moiety bound to the T2–T3 cluster [7, 8], so the absence of a band or a shoulder at 330 nm is expected. In the case of the mutants, the absence of this band is consistent with the X-ray crystal structures where a dioxygen molecule and a peroxide moiety are observed bound to the trinuclear cluster of the M502L and M502F mutants, respectively (Fig. 2e, f).

#### Structural characterization of M502L and M502F mutants

The M502L and the M502F mutants show the characteristic fold of the “as-isolated” protein [8]. It comprises three cupredoxin domains, a mononuclear type 1 copper centre localized in domain 3, and a trinuclear copper centre that is placed between domains 1 and 3. In the as-isolated structure of CotA the copper atom in the mononuclear type 1 copper centre has three strong ligands, two histidine residues and one cysteine residue, and a weak axial ligand, a methionine, which was mutated into a leucine and a phenylalanine, as described earlier. The polypeptide chain of both mutants was traced through ( $2F_o - F_c$  and  $F_o - F_c$ ) electron density maps, except for a region positioned at the protein surface (residues 89–96). In all the CotA structures refined so far, this region has always been poorly defined [6–8]. In addition, two residues (Asp187 and Leu425) systematically appear in the disallowed region of the Ramachandran plot [23]; however, these are well-defined residues located at the beginning of a  $3_{10}$  helix (Asp187) and in a  $\gamma$ -turn (Leu425). The T1 and trinuclear copper centres were readily positioned in the electron density maps, as well as the mutated residues (Fig. 2a, b).

In the M502L mutant, the position of Leu502 side chain does not differ significantly from that occupied by the methionine residue in the native protein; however, the  $C^{\delta 2}$ Leu502 atom is located further away (at 3.4 Å) from the type 1 copper (Table 2, Fig. 2c) and no longer coordinates to it, as observed in other laccases which have a leucine at that position. Overall, the geometry of the type 1 copper centre is maintained (Table 2, Fig. 2c), although some depletion of the copper anion is observed (occupancy 0.85). Likewise, in the M502F mutant the phenylalanine residue is positioned further away from the copper atom (Fig. 2b), and does not coordinate to it. The distance ( $C^{\delta 2}$ -Cu1 3.6 Å), in this case is slightly longer than that observed for the leucine mutant, but is within the range that is observed in other laccases that possess the same axial residue [24–26]. Again, the overall geometry of the type 1 copper centre is maintained (Table 2, Fig. 2d) and no significant differences were

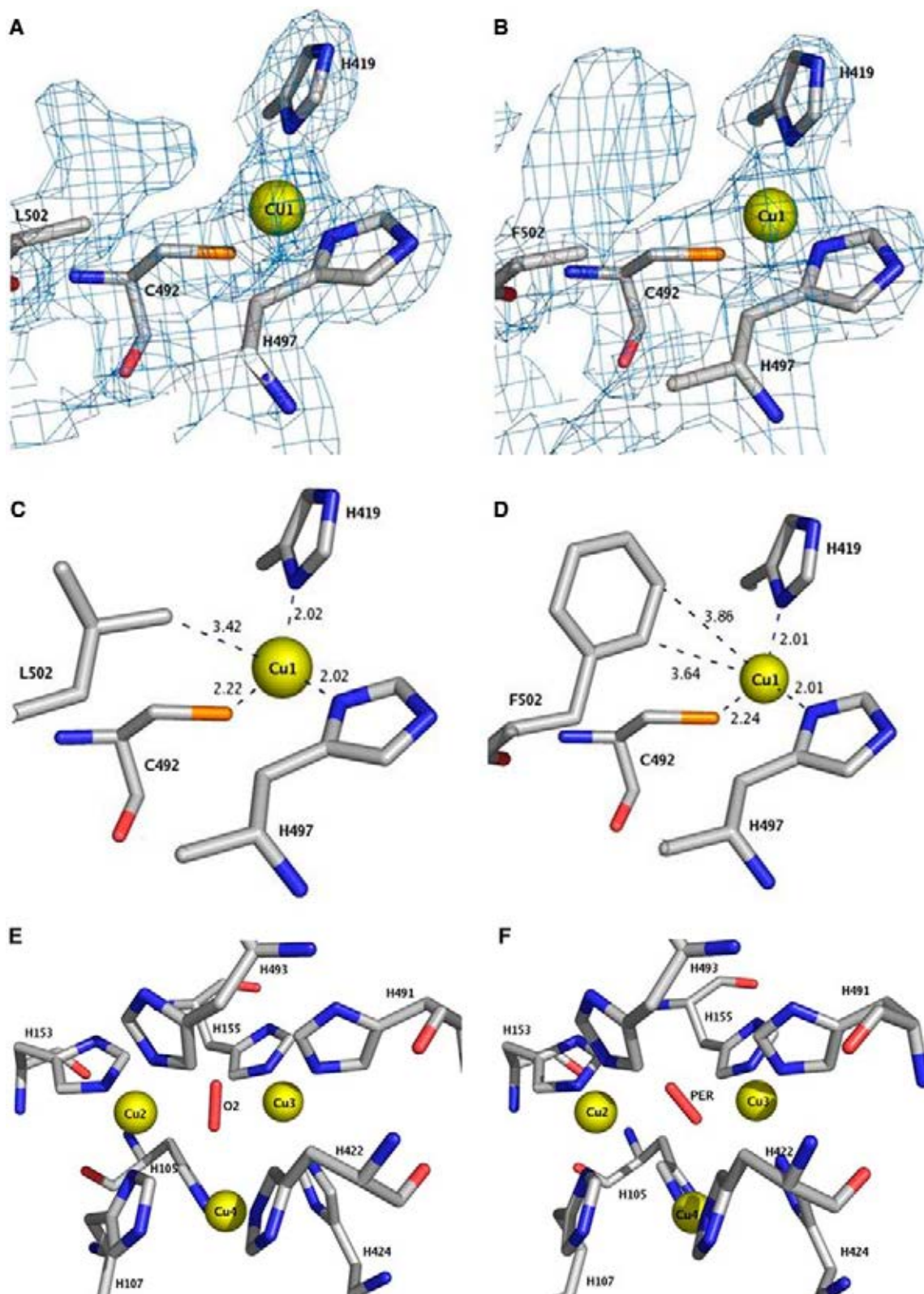


**Fig. 2** Detail of the type 1 copper centre with a section of the  $2F_o - F_c$  electron density map contoured at  $1\sigma$  and showing the mutated residue in M502L (**a**, **c**) and M502F (**b**, **d**); detail of the trinuclear centre in the M502L mutant (**e**) and in the M502F mutant (**f**)

identified in its neighbourhood. The structural comparison of both mutants with the as-isolated CotA showed that, apart from a region that is positioned close to the

mutated residue, all the polypeptide chain is invariant (Fig. 3). The slight movement of the mutated residue towards the protein surface, and away from the type 1

**Table 2** Bond distances at the copper centres

	CotA	M502L	M502F
<b>Mononuclear type 1 copper centre</b>			
T1 4th ligand	Met	Leu-CD2	Phe-CD2 (CE2)
Cu–ligand	3.2	3.4	3.6 (3.9)
Cu–His	H497, 1.98 H419, 2.02	H497, 2.02 H419, 2.02	H497, 2.01 H419, 2.01
Cu–Cys	2.22	2.22	2.24
Resolution (Å)	2.00	2.05	2.3
<b>Trinuclear copper centre</b>			
Cu2–Cu3	4.73	4.73	4.88
Cu2–Cu4	3.66	4.04	4.14
Cu3–Cu4	3.99	3.81	3.89
Cu2–O1	2.57	2.61	2.33
Cu2–O2	2.59	2.50	3.01
Cu3–O1	2.31	2.28	2.67
Cu3–O2	2.29	2.37	1.94
Cu4–O2	2.42	2.56	2.80
Cu4–w	2.98	2.92	2.77
O1–w	2.40	2.71	2.79
w–E498	2.86	2.48	2.74
Cu2–H493	2.13	2.05	2.05
Cu2–H153	2.08	2.03	2.01
Cu2–H107	2.07	2.00	2.01
Cu3–H155	2.11	2.02	2.01
Cu3–H491	2.03	1.99	2.00
Cu3–H424	2.04	1.99	1.99
Cu4–H105	1.96	1.96	1.94
Cu4–H422	2.03	1.95	1.97

copper atom, leads to a concerted movement of this region, pushing it away towards the solvent, and slightly increasing the exposure of the copper centre.

In both mutant structures a diatomic moiety was modelled between the two type 3 copper anions in the trinuclear centre. For the M502L mutant a dioxygen

moiety was modelled (O1–O2 distance 1.20 Å) (Fig. 2e) symmetrically positioned between the two copper atoms, as observed in the as-isolated structure of CotA [8]. In the M502F mutant a peroxide moiety was modelled (O1–O2 distance 1.45 Å), tilted with respect to the type 3 copper anions (Fig. 2f). This moiety is similar to that observed in the peroxide adduct [8] and constitutes another intermediate state in the mechanism of dioxygen reduction to water [8]. In the peroxide adduct, crystals of the as-isolated CotA were deliberately soaked with hydrogen peroxide. This was not the case for the M502F mutant and the occurrence of the peroxide intermediate must indicate that it is the most stable intermediate in the overall reaction cycle under the crystallization conditions used. The precise reasons why this state was isolated are not clear, since no substrate or reducing agent was deliberately added to the sample and there was no indication that radiation damage during X-ray data collection was significant.

#### Redox potential at the T1 site of wild-type and mutant proteins

The reduction of the T1 copper ion was measured by the disappearance of the “blue” absorbance band over 500–800 nm. The normalized amplitude of the absorption band measured at 600 nm as a function of the potential for the three enzymes is displayed in Fig. 4. The redox potentials of the T1 Cu site were determined to be 455, 548 and 515 mV for the wild type, M502L and M502F, respectively (Table 3). Thus, the replacement of the axial methionine residue by a leucine and a phenylalanine in

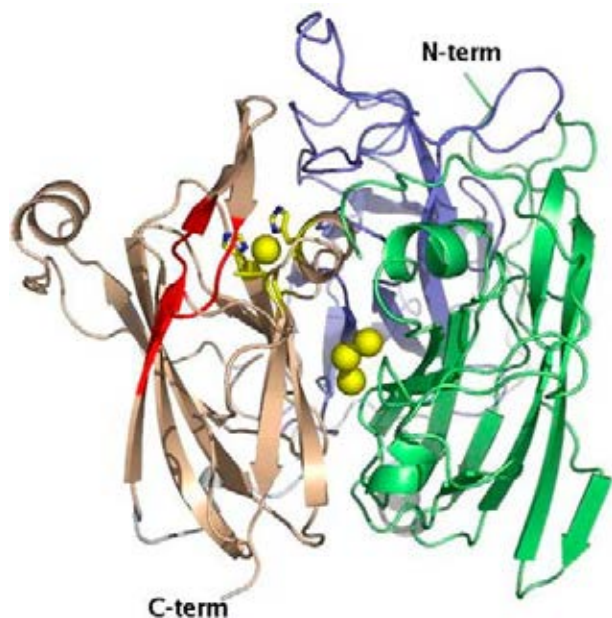


**Fig. 3** Representation of the three-dimensional structure of CotA with the cupredoxin domains coloured differently (domain 1 *green*, domain 2 *slate*, domain 3 *wheat*) and the variant region in *red* (M502L residues 371–377, 386–399; M502F residues 375–376, 387–389). Prepared with PyMol [27]

the CotA laccase leads to an increase of the redox potential by approximately 100 and 60 mV, respectively. The T1 Cu site of M502L and M502F (Fig. 2a–d) closely mimics the structural characteristics of the wild-type CotA laccase, displaying a flattened trigonal geometry in the absence of the fourth ligand. The redox potential increase should therefore be a direct consequence of this specific change to the axial ligand in the Cu centre and is most probably related to the stabilization of reduced state of the copper atom, Cu(I), by the elimination of the axial ligand; all the other parameters that are known to influence the redox potential, such as the solvent accessibility of the metal site, the charge dipole distribution around the copper, and the hydrogen bonds with the cysteine sulfur atom [11] appear to remain unchanged. Axial ligand mutations at T1 copper sites in other enzymes have been extensively studied and it has been recognized that they are a key factor in modulating the redox potential of blue copper sites in the range from approximately 100 to 200 mV [28–34].

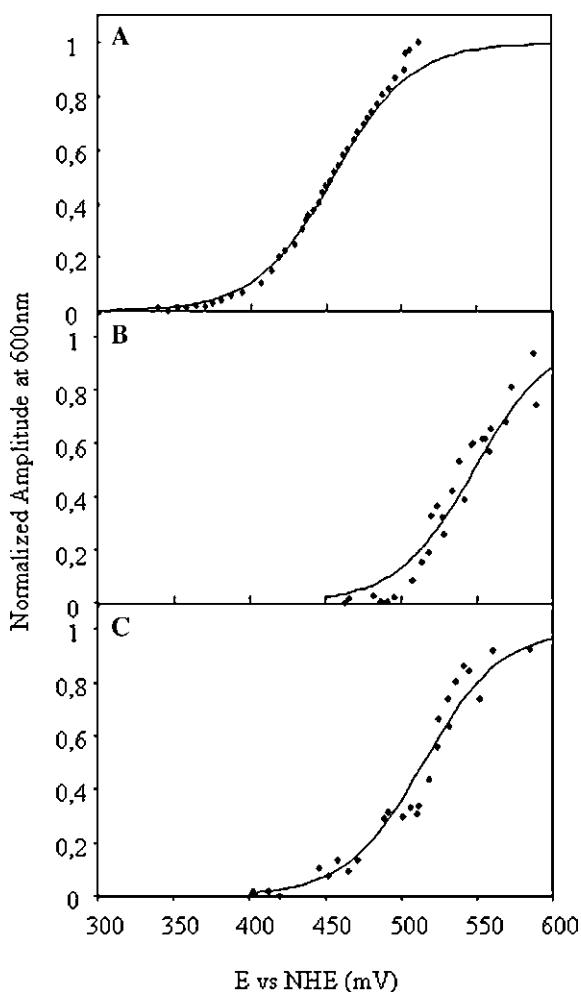


**Fig. 4** Redox titrations of wild type (a) and M502L (b) and M502F (c) mutants. The *solid lines* show the best fit of the experimental data given by one-electron Nernst curves

Catalytic properties of mutants as compared with the wild type

Four different reducing substrates, two non-phenolic, ABTS and  $K_4(FeCN_6)$ , and two phenolic, SGZ and 2,6-DMP, were used to identify specific changes in the catalytic properties of M502L and M502F mutants as compared with the wild-type enzyme. The wild-type and the mutant proteins exhibited maximal activity for ABTS and  $FeCN_6$  at pH 3 and for SGZ and 2,6-DMP at pH 7, displaying the typical monotonal decrease as pH increases for the non-phenolic substrates and a bell-shaped profile for the phenolic substrates (results not shown). Overall, the pH profiles of both single mutants were similar to those of the wild-type enzyme (results not shown). A comparison of the catalytic activities at the optimum pH for the wild-type and the mutant enzymes is shown in Table 3. These mutations did not result in major alterations regarding the  $K_m$  for the different substrates; values that differ as much as threefold were calculated for all the substrates tested. It was not expected that the mutations would have major effects on the substrate binding site, and indeed no major changes in the affinity for different substrates were observed. Significant changes were found, however, for both mutants, in the values of  $k_{cat}$  calculated. The M502L mutant exhibits a twofold to fourfold decrease in  $k_{cat}$  towards the oxidation of all the non-phenolic and phenolic substrates tested. Mutant M502F presents a tenfold decrease in  $k_{cat}$  towards the oxidation of the non-phenolics ABTS and  $FeCN_6$  compared with the wild-type enzyme and an 1,840-fold and 665-fold decrease in  $k_{cat}$  towards the oxidation of the phenolic substrates, implying that its ability to oxidize phenolic substrates is highly reduced. The large decrease in the catalytic activity of the M502F mutant towards phenolic substrates whose oxidation accompanies proton release, in contrast to the oxidation of non-phenolic substrates, is not understood at present. One result that appears outstanding, however, is that no direct correlation was found between the redox potentials calculated for the mutant enzymes and the oxidation rates of the substrates tested. Both mutants exhibited higher redox potentials than the wild-type CotA laccase and lower turnover rates. The parameter  $k_{cat}$  is reflective of the enzymatic rate-limiting step that was shown to be the substrate oxidation under steady-state conditions [9]. For an electron-transfer reaction its rate ( $k_{ET}$ ) is mainly determined, according to Marcus theory, by three factors: the donor–acceptor electronic coupling ( $H_{AD}$ ), where the exact geometry of the protein matrix has an important role; the redox potential ( $E^0$ ); and the reorganization energy ( $\lambda$ ), which also depends on the structure and the dynamics of the protein [35]. The higher redox potential determined for both mutants would appear to favour an increased reaction velocity, as  $k_{ET}$  is a major component of the parameter  $k_{cat}$  [9]. In the present case, we can hypothesize that mutations could have affected the electronic tunnelling and/or the reor-

**Table 3** Redox potential and substrate specificity of the wild-type CotA laccase and mutant enzymes

	$E^0$ (mV)	ABTS		$K_4(\text{FeCN}_6)$		SGZ		2,6-DMP	
		$K_m$ ( $\mu\text{M}$ )	$k_{\text{cat}}$ ( $\text{s}^{-1}$ )	$K_m$ ( $\mu\text{M}$ )	$k_{\text{cat}}$ ( $\text{s}^{-1}$ )	$K_m$ ( $\mu\text{M}$ )	$k_{\text{cat}}$ ( $\text{s}^{-1}$ )	$K_m$ ( $\mu\text{M}$ )	$k_{\text{cat}}$ ( $\text{s}^{-1}$ )
Wild type	455	87 ± 10	22.4 ± 0.9	69 ± 2	54.5 ± 1.0	10 ± 1	18.4 ± 0.4	60 ± 17	6.65 ± 0.5
M502L	548	89 ± 5	10.6 ± 0.24	27 ± 5	20.9 ± 0.4	9 ± 1	7.4 ± 2.2	145 ± 16	1.55 ± 0.1
M502F	515	49 ± 4	0.26 ± 0.003	67 ± 4	5.5 ± 0.04	8 ± 1	0.01 ± 0.003	35 ± 7	0.01 ± 0.001

ABTS 2,2'-azinobis(3-ethylbenzothiazoline-6-sulfonic acid), SGZ syringaldazine, 2,6-DMP 2,6-dimethoxyphenol

ganization energy of the two electron-transfer processes (from the substrate to the T1 centre and from this to the trinuclear site) to find possible reasons for discrepancies in the overall velocity of reactions in the different proteins studied. It is possible that the replacement of methionine by leucine and phenylalanine, leading to elimination of a dipole, could contribute to the electrostatic destabilization of the reduced form of the T1 copper site [36]. The accommodation of an electron at this site would therefore require an increase in the reorganization energy, which in turn could result in lower  $k_{\text{ET}}$  and thus lower turning number values in the mutant proteins. However, none of these possibilities can be clearly investigated here.

### Stability studies

The thermodynamic stability and characterization of the unfolding of CotA induced by GdnHCl was achieved by using different spectroscopic techniques and activity measurements. Figure 5a shows the thermodynamic stability of the tertiary structure of CotA wild type as assessed by fluorescence. The wavelengths at the emission maxima reflect clearly the exposure of tryptophan residues to the high polarity of water at the surface of the protein upon unfolding [37]. The CotA tertiary structure is very stable, displaying a GdnHCl concentration of 4.6 M at the midpoint (where 50% of the molecules are unfolded), and the native state is more stable than the unfolded state by 10 kcal/mol at 25 °C (Table 4). The unfolding process was accurately described according to a two-state process with native and unfolded states being the only ones that accumulate significantly ( $\text{N} \leftrightarrow \text{U}$ ). Far-UV circular dichroism was also used to assess the unfolding of the secondary structure (data not shown). The CotA secondary structure unfolds at the same GdnHCl concentration as unfolding of the tertiary structure was observed (4–6 M) but accurate quantification was not possible. CotA has a relatively low content of the secondary structure, mostly  $\beta$ -sheets (3.5% of  $\alpha$ -helices and 37% of  $\beta$ -sheets, PDB entry 1GSK) which display a low mean residue ellipticity [38].

Thermodynamic stability was also assessed by activity measurements and absorbance at 600 nm to probe CotA function and copper binding at T1, respectively (Fig. 5b). The use of a multidimensional approach that

measures changes at the level of tertiary structure (fluorescence), secondary structure (circular dichroism in the far-UV), function (activity) and copper binding/coordination (absorbance at 600 nm) provides information on the heterogeneity of protein population in equilibrium. Since both the activity and the absorbance at 600 nm depend on copper bonding to T1 and they follow approximately the same trend upon increased GdnHCl concentrations, the decays of activity and absorbance at 600 nm were accurately fitted according to a two-state process describing an equilibrium between

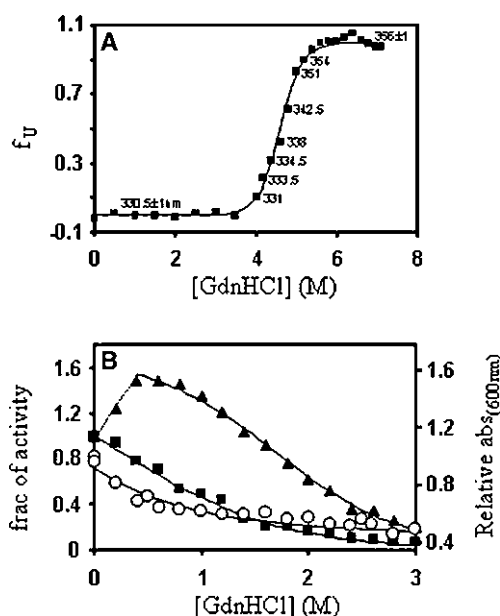


**Fig. 5 a** Fraction of wild-type CotA laccase unfolded ( $f_U$ ) by guanidinium hydrochloride (GdnHCl) as measured by fluorescence emission. The solid line is the fit according to the equation  $f_U = \exp(-\Delta G^0/RT) / (1 + \exp(-\Delta G^0/RT))$ , which assumes the equilibrium  $\text{N} \leftrightarrow \text{U}$  and was derived from Eqs. 1, 2, 3, 4 and 5 and the numbers are the wavelengths at the emission maximum. **b** Change in activity in the absence (squares) and presence (triangles) of copper (copper-to-CotA ratio 4:1) and change in absorbance at 600 nm (circles) at increasing GdnHCl concentrations. The solid lines are the fits according to the equation  $y = y_N + y_{\text{N(no copper)}} \exp(-\Delta G^0/RT) / (1 + \exp(-\Delta G^0/RT))$ , which assumes the equilibrium  $\text{N} \leftrightarrow \text{N}_{\text{no copper}}$  and was derived from Eqs. 1, 2, 3, 4 and 5, where  $y_N$  and  $y_{\text{N(no copper)}}$  are the relative activity or the absorbance for the native state and native state without copper, respectively. In the presence of copper, an initial increase in activity which cannot be fitted according to the process of copper loss is highlighted by a dashed line to help visual inspection

**Table 4** Thermodynamic stability of the tertiary structure of CotA wild type and mutants M502L and M502F as assessed by fluorescence spectroscopy

	$\Delta G_{1st}^{0\text{ water}}$ (kcal/mol)	$m_{1st}$ (kcal/mol M)	Midpoint <sub>1st</sub> (M)	$\Delta G_{2nd}^{0\text{ water}}$ (kcal/mol)	$m_{2nd}$ (kcal/mol M)	Midpoint <sub>2nd</sub> (M)
CotA wild type	10.0 ± 0.1	2.2 ± 0.0	4.6 ± 0.1	–	–	–
M502L	1.4 ± 0.0	0.7 ± 0.1	1.9 ± 0.2	7.1 ± 0.6	1.4 ± 0.1	5.0 ± 0.0
M502F	1.4 ± 0.1	0.9 ± 0.1	1.6 ± 0.0	6.2 ± 0.5	1.3 ± 0.2	4.8 ± 0.2

*1st* first transition, meaning from N to U for the wild type and from N to I for mutants; *2nd* second transition, meaning from I to U, which exists only for mutants

the native state with copper and the native state with no copper at T1 ( $N \leftrightarrow N_{\text{no copper}}$ ). Parameters describing this equilibrium assessed by activity are shown in Table 5. The process of copper depletion from T1 and the concomitant loss of activity are not related to the unfolding of secondary and tertiary structures as they occur at much lower GdnHCl concentrations. Copper depletion is the key event in the inactivation and thus for the thermodynamic stability of CotA wild type. Even in buffer (at 0 M GdnHCl), the native state with copper is only marginally more stable than the native state with no copper at T1 (0.2 kcal/mol), leading to the accumulation of around 43% of CotA molecules without copper. This point is fully supported by measuring the equilibrium between N and  $N_{\text{no copper}}$  in the presence of copper in solution (Fig. 5b, Table 5). CotA wild type is able to incorporate copper with an initial increase in GdnHCl concentration up to 0.4 M, leading to an increase in activity. The parameters obtained from the fit also reflect copper uptake as the equilibrium is shifted towards N in the presence of copper and the energy gap between N and  $N_{\text{no copper}}$  increases to 1.4 kcal/mol. Clearly, the loss of the CotA enzymatic activity correlates to T1 copper depletion, and not with global unfolding of secondary and tertiary structures. The thermodynamic parameters shown in Table 4 for the wild-type protein characterize the transition from N with no copper at T1 to U as copper is lost at much lower GdnHCl concentrations. These results appear to contradict previous results where it was observed that the unfolding of three fungal laccases coincides with their inactivation [38], but are in accordance with results obtained for the thermal denaturation of the plant *Rhus*

*vernificera* laccase [40] and in the fungal *Coriolus hirsutus* and *Coriolus zonatus* laccases [41], where copper is lost at relatively low temperatures and where global unfolding of secondary and tertiary structures could not still be detected.

The mutations M502L and M502F have a profound impact on the stability of CotA. Only the stability of M502L is shown in Fig. 6 but the mutant M502F shows basically the same behaviour (Table 4). First, the unfolding of the tertiary structure is clearly a non-two-state process. The accumulation of an intermediate state (I) in-between N and U that occurs at low GdnHCl concentration (at 1.9 M GdnHCl, 50% of molecules are in the I state) allows the accurate fit of the unfolding process. The I state accumulates at low GdnHCl concentration because the native state is more stable than the I state by only 1.4 kcal/mol. Tryptophan residues are partially exposed to water in the I state as shown by the wavelength of the emission maximum, indicating that the I state is a partially unfolded state. As the stability of the I state is close to that of the native state, the conversion from I to U occurs only at high GdnHCl concentrations and is thermodynamically similar to the conversion of N to U in the wild-type protein. The term  $m$ , which is the cooperativeness of the transition, contains interesting information as it is a measure of the degree of unfolding for a given transition [42]. The global unfolding of the wild-type protein is characterized by an  $m$  value of 2.2 kcal/mol M, which is equal to the overall unfolding transition from N to U for the mutants ( $m_{1st} + m_{2nd}$  is 2.1 and 2.2 kcal/mol M for M502L and M502F, respectively). This indicates that the

**Table 5** Thermodynamic stability of CotA wild type and mutants M502L and M502F as assessed by activity

	$\Delta G_{1st}^{0\text{ water}}$ (kcal/mol)	$m_{1st}$ (kcal/mol M)	Midpoint <sub>1st</sub> (M)
CotA wild type	0.2 ± 0.0	0.7 ± 0.1	0.3 ± 0.1
CotA wild type + copper (1:4)	1.4 ± 0.4	0.9 ± 0.1	1.5 ± 0.3
M502L	0.3 ± 0.7	0.7 ± 0.1	0.4 ± 0.9
M502L + copper (1:4)	1.0 ± 0.4	1.5 ± 0.5	0.7 ± 0.1
M502F + copper (1:8)	−0.1 ± 0.8	0.8 ± 0.1	<sup>a</sup>
M502F + copper (1:70)	0.8 ± 0.3	1.2 ± 0.1	0.6 ± 0.1

Activity was measured in the absence and presence of copper (1:4 ratio of protein to copper) for wild type and M502L and in the presence of two copper concentrations (1:8 and 1:70 ratios of protein to copper) for the M502F mutant

*1st* first transition, which is from N with copper to N without copper for the wild type. For mutants the intermediate I accumulates at very low GdnHCl concentration and the first transition might be from N to  $I_{\text{no Cu}}$

<sup>a</sup>At 0 M GdnHCl more than 50% of the molecules have no copper at T1 ( $\Delta G_{1st}^{0\text{ water}}$  is negative) and therefore the midpoint cannot be defined

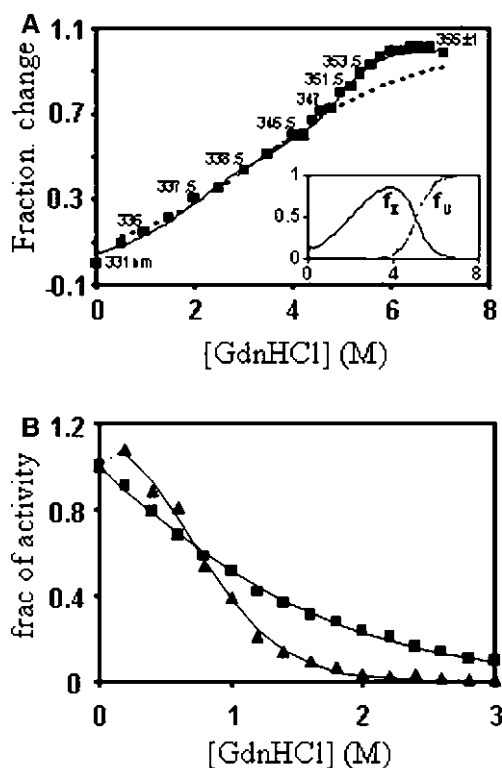


**Fig. 6** **a** Fractional change of the fluorescence signal from the M502L mutant induced by GdnHCl as measured by fluorescence emission. The *dashed line* is the fit according to a two-state model ( $N \leftrightarrow U$ , see Eqs. 1, 2, 3, 4, 5) and the *solid line* is the fit according to a three-state model ( $N \leftrightarrow I \leftrightarrow U$ ) using Eq. 13. *Numbers* are the wavelengths at the emission maximum showing that the CotA M502L mutant initiates unfolding (accumulation of I) at very low GdnHCl concentrations. The *inset* shows precisely the accumulation of I and its disappearance to give the unfolded state with the increase in GdnHCl concentration, calculated according to Eqs. 14 and 15, respectively. **b** Change in activity of the CotA M502L mutant in the absence (*squares*) and presence (*triangles*) of copper (copper-to-CotA ratio 4:1) at increasing GdnHCl concentrations. The *solid lines* are the fits according to the equation  $y = y_N + y_{N(\text{no copper})} \exp(-\Delta G^0/RT) / (1 + \exp(-\Delta G^0/RT))$  derived from Eqs. 1, 2, 3, 4 and 5, where  $y_N$  and  $y_{N(\text{no copper})}$  are the relative activities for the native state and the native state without copper, respectively. In the presence of copper, a small increase in activity which cannot be fitted according to the process of copper loss is highlighted by a *dashed line* to help visual inspection

structure of N is basically the same for wild-type and mutant proteins at the level of exposure to the solvent (as it is not expected that the U state will change upon mutation). This observation is fully supported by the invariant three-dimensional structures obtained for both mutants (see earlier) and by the invariant emission maximum of tryptophan residues (approximately 331 nm). Nevertheless, our results indicate that the native overall structure of the mutant enzyme is less stable when compared with the structure of the wild-type enzyme. In fact, global unfolding of the wild type is characterized by a  $\Delta G^0_{\text{water}}$  of 10 kcal/mol, but the free-energy gap between N and U for the mutants (given by  $\Delta G^0_{1\text{st}} + \Delta G^0_{2\text{nd}}$ ) is lower for M502L (8.5 kcal/mol) and even lower for M502F (7.6 kcal/

mol), the most destabilized structure. The mutant M502L also loses activity at very low GdnHCl concentrations in exactly the same way as the wild type (the midpoints are 0.4 and 0.3 M, respectively; Table 5). Copper uptake however was not significant at low GdnHCl concentrations and only a very small increase in the activity was observed (Fig. 6b). Probably the I state that accumulates at low GdnHCl concentration cannot incorporate copper from the solution. For the mutant M502F, copper uptake was even more compromised and the equilibrium was further shifted to  $N_{\text{no copper}}$ , leading to  $\Delta G^0_{\text{water}}$  being negative and more than 50% of the protein molecules having no copper at T1 (Table 5). It appears that the mutations M502L and M502F have destabilized the conformation of the T1 site without causing gross structural changes in the tertiary structure. These mutations may have created a “hot spot” where partial unfolding that leads to accumulation of the I state is probably initiated. The slight movement of the mutated residues towards the protein surface, and away from the type 1 copper atom, leads to a concerted movement of the region positioned close to the mutated residues (Fig. 3 and previous discussion), pushing it away towards the solvent, and opening the copper centre. The loss of stability observed for the mutant proteins may be correlated with this structural change. Indeed, the weakening of the copper coordination and subtle alterations in the interconnections of the residues could lead to decreasing stabilization of the centre and thus of the whole structure.

## Concluding remarks

Integrated studies have been undertaken on the CotA laccase from *B. subtilis* after site-directed mutagenesis on the catalytic mononuclear T1 copper site. The role of the T1 site within the multicopper oxidases is related to the long-range intramolecular electron transfer, shuttling the electrons from the reduced substrate to the trinuclear centre, where  $O_2$  is reduced to water. The X-ray analysis of mutants has shown that replacement of the axial Cu methionine ligand by the non-coordinating hydrophobic residues leucine and phenylalanine did not lead to major structural changes in the geometry of the centre or in the overall fold of the enzyme. Thus, an increase of the redox potential of the both mutant enzymes by as much as 100 mV has been attributed to the weakening in the T1 Cu coordination. Nevertheless, no direct correlation was found between the redox potentials calculated for the M502L and M502F enzymes and the oxidation rates of several non-phenolic and phenolic substrates tested, as lower turnover rates were calculated for both mutants when compared with the wild-type enzyme. Furthermore, the mutations in the axial ligand have a profound impact on the thermodynamic stability of the enzyme; the accumulation of an intermediate state in-between the native and unfolded states occurs at low concentrations

of denaturant, in contrast with the two-state unfolding process of the wild-type enzyme. Mutant M502F is more severely compromised in its biological function than the M502L mutant. The aromatic phenylalanine residue is larger than leucine or methionine residues and is positioned at a distance slightly further from the T1 Cu than leucine. This resulted in a higher local instability of the structure as shown by the smaller free-energy gap calculated between the native and unfolded states and also by the decreased ability to incorporate copper from solution as compared with the wild type or the M502L mutant. These variations should be related to the radical drop in the catalytic ability. Our results indicate that copper depletion is a key event in the inactivation and thus in the thermodynamic stability of CotA laccase. The enzyme loses copper from the T1 site and the activity decreases abruptly at very low GdnHCl concentrations, compared with those needed to unfold secondary and tertiary structures, indicating that copper is the first parameter affecting the enzyme thermodynamic stability. In the present work it was shown that subtle rearrangements in the coordination sphere of the T1 copper result in major loss of function regarding the catalytic as well as the overall stability of the enzyme, raising new questions regarding our understanding of the structure and function of the oxidative copper site of the blue multicopper oxidases.

**Acknowledgements** We would like to thank our colleagues at the Instituto de Tecnologia Química e Biológica, Universidade Nova de Lisboa (ITQB-UNL), Cláudio M. Soares, António M. Baptista and Manuela M. Pereira for support and useful discussions. We would also like to thank João Carita for help with the cell growth in the Organic Fermentation Unit at the ITQB-UNL. The ITQB-UNL and the Fundação para a Ciência e a Tecnologia provided the resources necessary for this research. All X-ray data were collected at the European Synchrotron Radiation Facility, Grenoble, France, with the kind assistance of the scientists responsible for the operation of beam line ID29.

## Appendix

The thermodynamic stability of CotA wild type monitored by fluorescence was analysed according to a two-state process ( $N \leftrightarrow U$ ) using the following equations:

$$y = y_N f_N + y_U f_U, \quad (1)$$

$$K_{(U-N)} = f_U / f_N, \quad (2)$$

$$\Delta G_{(U-N)}^0 = -RT \ln K_{(U-N)}, \quad (3)$$

$$y = \frac{\left( y_N + y_I \exp\left(\frac{-\Delta G_{(I-N)}^{0\text{water}} + m_{(I-N)}[\text{GdnHCl}]}{RT}\right) + y_U \exp\left(\frac{-\Delta G_{(I-N)}^{0\text{water}} + m_{(I-N)}[\text{GdnHCl}]}{RT}\right) \exp\left(\frac{-\Delta G_{(U-I)}^{0\text{water}} + m_{(U-I)}[\text{GdnHCl}]}{RT}\right) \right)}{\left( \exp\left(\frac{-\Delta G_{(I-N)}^{0\text{water}} + m_{(I-N)}[\text{GdnHCl}]}{RT}\right) + 1 + \exp\left(\frac{-\Delta G_{(I-N)}^{0\text{water}} + m_{(I-N)}[\text{GdnHCl}]}{RT}\right) \exp\left(\frac{-\Delta G_{(U-I)}^{0\text{water}} + m_{(U-I)}[\text{GdnHCl}]}{RT}\right) \right)}. \quad (13)$$

$$\Delta G_{(U-N)}^0 = \Delta G_{(U-N)}^{0\text{water}} - m_{(U-N)}[\text{GdnHCl}] \quad (4)$$

and

$$[\text{GdnHCl}]_{50\%} = \Delta G_{(U-N)}^{0\text{water}} / m_{(U-N)}, \quad (5)$$

where N and U are native and unfolded CotA, respectively,  $y$  is the fluorescence signal,  $f$  is the fraction of CotA molecules with a given conformation,  $K$  is the equilibrium constant,  $\Delta G^0$  is the standard free energy,  $m_{(U-N)}$  is the linear dependence of  $\Delta G^0$  on GdnHCl concentration and  $[\text{GdnHCl}]_{50\%}$  is the GdnHCl concentration for  $\Delta G^0 = 0$ .  $y_N$  and  $y_U$  were calculated directly from the pretransition and posttransition regions according to a linear dependence.

The thermodynamic stability evaluated by activity measurements and the absorbance at 600 nm are dependent on copper loss from T1. Therefore Eqs. 1, 2, 3, 4 and 5 were used but considering that the two-state process assessed by these two techniques is the establishment between the native state with copper bound at T1 and the native state with no copper at T1 ( $N \leftrightarrow N_{(\text{no copper})}$ ).

The thermodynamic stability of CotA M502L and M502F mutants monitored by fluorescence could only be accurately fitted according to a three-state process, with the accumulation of an intermediate state in-between N and U ( $N \leftrightarrow I \leftrightarrow U$ ). The following equations were used:

$$y = y_N f_N + y_I f_I + y_U f_U, \quad (6)$$

$$K_{(I-N)} = f_I / f_N, \quad (7)$$

$$K_{(U-I)} = f_U / f_I, \quad (8)$$

$$\Delta G_{(I-N)}^0 = -RT \ln K_{(I-N)}, \quad (9)$$

$$\Delta G_{(U-I)}^0 = -RT \ln K_{(U-I)}, \quad (10)$$

$$\Delta G_{(I-N)}^0 = \Delta G_{(I-N)}^{0\text{water}} - m_{(I-N)}[\text{GdnHCl}] \quad (11)$$

and

$$\Delta G_{(U-I)}^0 = \Delta G_{(U-I)}^{0\text{water}} - m_{(U-I)}[\text{GdnHCl}], \quad (12)$$

where  $y_N$  was considered to be the fluorescence signal at 0 M GdnHCl (this assumption was confirmed by the fluorescence emission maximum) and  $y_U$  was calculated directly from the posttransition regions according to a linear dependence.

Combining Eqs. 6, 7, 8, 9, 10, 11 and 12, we fitted the fluorescence signal (and therefore fractional change of fluorescence signal) according to Eq. 13:

The fits were carried out by varying values of  $y_I$ ,  $\Delta G_{(I-N)}^{0 \text{ water}}$ ,  $m_{(I-N)}$ ,  $\Delta G_{(U-I)}^{0 \text{ water}}$  and  $m_{(U-I)}$  with the Origin software using the non-linear curve-fit option. Combination of Eqs. 6, 7 and 8 leads to

$$f_I = \frac{K_{(I-N)}}{1 + K_{(I-N)} + K_{(I-N)}K_{(U-I)}} \quad (14)$$

and

$$f_U = \frac{K_{(I-N)}K_{(U-I)}}{1 + K_{(I-N)} + K_{(I-N)}K_{(U-I)}}. \quad (15)$$

---

## References

- Messerschmidt A (1997) Multi-copper oxidases. World Science, Singapore
- Lindley PF (2001) In: Bertini I, Sigel A, Sigel H (eds) Multi-copper oxidases. Handbook on metalloproteins. Dekker, New York, pp 763–811
- Xu F (1999) In: Flickinger MC, Drewn SW (eds) Encyclopedia of bioprocess technology: fermentation, biocatalysis and bio-separation. Wiley, New York, pp 1545–1554
- Gianfreda L, Xu F, Bollag J-M (1999) Bioremediation J 3:1–25
- Martins LO, Soares CM, Pereira MM, Teixeira M, Costa T, Jones GH, Henriques AO (2002) J Biol Chem 277:18849–18859
- Enguita FJ, Martins LO, Henriques AO, Carrondo MA (2003) J Biol Chem 278:19416–19425
- Enguita FJ, Marçal D, Martins LO, Grenha R, Henriques AO, Lindley PF, Carrondo MA (2004) J Biol Chem 279:23472–23476
- Bento I, Martins LO, Lopes GG, Arménia MA, Lindley PF (2005) Dalton Trans 21:3507–3513
- Xu F (1996) Biochemistry 35:7608–7614
- Solomon EI, Sundaram UM, Machonkin TE (1996) Chem Rev 96:2563–2605
- Karlin S, Zhu SZY, Karlin KD (1997) Proc Natl Acad Sci USA 94:14225–14230
- Otwinowski Z, Minor W (1997) In: Carter CW Jr, Sweet RM (eds) Methods in enzymology, macromolecular crystallography, vol 276. Academic, New York, pp 307–326
- CCP4 (1994) Acta Crystallogr Sect D 50:760–763
- Murshudov GN, Vagin AA, Lebedev A, Wilson KS, Dodson EJ (1999) Acta Crystallogr Sect D 55:247–255
- Emsley P, Cowtan K (2004) Acta Crystallogr Sect D 60:2126–2132
- Ramakrishnan C, Ramachandran GN (1965) Biophys J 5:909–933
- Laskowski RA, MacArthur MW, Moss DS, Thornton JM (1993) J Appl Crystallogr 26:283–291
- Schneider TR (2002) Acta Crystallogr Sect D 58:195–208
- Bradford MM (1976) Anal Biochem 72:248–254
- Eftink MR (1994) Biophys J 66:482–501
- Monsellier E, Bedouelle H (2005) Protein Eng Des Sel 18:445–456
- Brenner AJ, Harris ED (1995) Anal Biochem 226:80–84
- Ramachandran GN, Sasisekharan V (1968) Adv Protein Chem 23:283–437
- Ducros V, Brzozowski AM, Wilson KS, Ostergaard P, Schneider P, Svendsen A, Davies GJ (2001) Acta Crystallogr Sect D 57:333–336
- Hakulinen N, Kiiskinen LL, Kruus K, Saloheimo M, Paananen A, Koivula A, Rouvinen J (2002) Nat Struct Biol 9:601–605
- Garavaglia S, Cambria MT, Miglio M, Ragusa S, Iacobazzi V, Palmieri F, D'Ambrosio C, Scaloni A, Rizzi M (2004) J Mol Biol 342:1519–1531
- DeLano WL (2002) The PyMOL molecular graphics system. DeLano Scientific, San Carlos
- Xu F, Berka RM, Wahleithner JA, Nelson BA, Shuster JR, Brown SH, Palmer AE, Solomon EI (1998) Biochem J 334:63–70
- Xu F, Palmer AE, Yaver DS, Berka RM, Gambeta GA, Brown SH, Solomon EI (1999) J Biol Chem 274:12372–12375
- Palmer AE, Randall DW, Xu F, Solomon EI (1999) J Am Chem Soc 121:7138–7149
- Pascher T, Karlsson BG, Nordling M, Malmström BG, Vänngård T (1993) Eur J Biochem 212:289–296
- Hall JF, Kanbi LD, Strange RW, Hasnain SS (1999) Biochemistry 38:12675–12680
- Diederix REM, Canters GW, Dennison C (2000) Biochemistry 39:9551–9560
- Kataoka K, Kitagawa R, Inoue M, Naruse D, Sakurai T, Huang H-W (2005) Biochemistry 44:7004–7012
- Moser CC, Dutton PL (1996) In: Bendall DS (ed) Protein electron transfer. Bios Scientific, Oxford, pp 1–21
- Warshel A (1978) Proc Natl Acad Sci USA 75:5250–5254
- Lakowicz JR (1999) Principles of fluorescence spectroscopy. Kluwer/Plenum, New York
- Kelly SM, Price NC (1997) Biochim Biophys Acta 1338:161–185
- Bonomo RP, Cennamo G, Purrello R, Santoro AM, Zappala RJ (2001) Inorg Chem 39:67–75
- Agostinelli E, Cervoni L, Giartosio A, Morpurgo L (1995) Biochem J 306:697–702
- Koroleva OV, Stepanova EV, Binukov VI, Timofeev VP, Pfeil W (2001) Biochim Biophys Acta 1547:397–407
- Fersht A (1999) Structure and mechanism in protein science. Freeman, New York